Signal Amplification Between G$\beta\gamma$ Release and PI3Kγ-Mediated PI(3,4,5)P_3 Formation Monitored by a Fluorescent G$\beta\gamma$ Biosensor Protein and Repetitive Two Component Total Internal Reflection/Fluorescence Redistribution after Photobleaching Analysis[†]

Astrid Tannert,[‡,§] Philipp Voigt,[‡] Steffen Burgold,[‡,||] Sebastian Tannert,[⊥] and Michael Schaefer*[,‡,§]

Department of Molecular Pharmacology and Cell Biology, Neurowissenschaftliches Forschungszentrum, Charité—Universitätsmedizin Berlin, Berlin, Germany, and PicoQuant GmbH, Berlin, Germany

Received April 4, 2008; Revised Manuscript Received August 27, 2008

ABSTRACT: Phosphoinositide 3-kinase γ (PI3Kγ) is activated by G$\beta\gamma$ release after stimulation of Gα_i-coupled receptors, involving a recruitment of the enzyme to the plasma membrane via interaction of the regulatory subunit p101 or p87 with G$\beta\gamma$. The receptor-mediated release of G$\beta\gamma$ was, however, insufficient to elicit a translocation of p101 observable by classical fluorescence microscopy approaches. Since the mobilities of plasma membrane-associated and cytosolic proteins differ strongly, small changes in the amount of plasma membrane association should be detectable by an altered diffusional behavior. Here, changes in mobility were monitored by fluorescence redistribution after photobleaching (FRAP) which was repetitively applied before and after stimulation of cells. To combine the advantages of total internal reflection (TIR) illumination, which preferentially excites fluorophors located at or near the plasma membrane, with that provided by the mobility information, we developed a combined TIR/FRAP setup which enabled us to point bleach parts of an image that was observed under TIR illumination. For FRAP data analysis, we introduce a convolution-based method and a global two component model. Using this TIR/FRAP approach, an increased plasma membrane association of the fluorescent G$\beta\gamma$-binding domain of p101 after G$\beta\gamma$ release by G protein-coupled receptor stimulation could be detected and quantified. By comparing the translocation efficiency of this domain with that of YFP-GRP1(PH), a biosensor for the PI3Kγ product PI(3,4,5)P_3, we evaluate the signal amplification between G$\beta\gamma$ release and PI(3,4,5)P_3 formation after activation of Gα_i-coupled receptors.

Phosphoinositide 3-kinases (PI3Ks)[1] comprise a family of lipid kinases that phosphorylate the 3′ position of inositol in phosphoinositides and thereby form lipid second messengers. By recruiting effector proteins that carry specific lipid binding domains to cellular membranes, they are involved in the regulation of a variety of cellular functions such as chemotaxis, proliferation, cell growth, metabolism, differentiation, and survival (*1, 2*). The receptor-activated class I PI3Ks are heterodimeric proteins containing a catalytic and a regulatory subunit. Their major product is phosphatidylinositol(3,4,5)-trisphosphate (PI(3,4,5)P_3), which is recognized by specific pleckstrin homology (PH) domains. The PH domain of GRP1 has been widely used to detect the generation of PI(3,4,5)-P_3 (*3, 4*). GFP-tagged GRP1(PH) serves as a biosensor which translocates from the cytosol to the plasma membrane indicating phosphoinositide 3-kinase activity in vivo (*3, 5*).

Class I PI3Ks are subdivided into class I_A and I_B, the former being activated by receptor tyrosine kinases. In contrast, PI3Kγ, the only member of the class I_B PI3K family, is activated by the release of G$\beta\gamma$ following activation of G protein-coupled receptors (GPCR). PI3Kγ activation plays a key role in cardiovascular regulation and in immune responses, e.g. by recruiting neutrophils to sites of inflammation (*6*).

PI3Kγ contains a p110γ catalytic and a p101 or p84/p87^{PIKAP} regulatory subunit (*7*−*9*). Interaction of PI3Kγ with G$\beta\gamma$ involves both the catalytic and the regulatory subunits. The regulatory p101 subunit bears a high affinity G$\beta\gamma$-binding domain and serves in recruiting PI3Kγ to the plasma membrane (*5*). Mapping of p101 identified the amino acids 650−850 as the G$\beta\gamma$ binding site of this subunit (*10*). In

[†] This work was supported by the Deutsche Forschungsgemeinschaft (FOR806, Schae941/2-1).

* Corresponding author. Tel.: +49 341 97 24600. Fax: +49 341 97 24609. E-mail: michael.schaefer@medizin.uni-leipzig.de.

[‡] Charité—Universitätsmedizin Berlin.

[§] Present address: Rudolf-Boehm-Institut für Pharmakologie and Toxikologie, Universität Leipzig, Härtelstrasse 16-18, D-04107 Leipzig, Germany.

[||] Present address: Institut für Neuropathologie, Zentrum für Neuropathologie and Prionforschung (ZNP), Ludwig-Maximilians-Universität München, München, Germany.

[⊥] PicoQuant GmbH.

[1] Abbreviations: AOI, area of interest; AOTF, acousto-optic tunable filter; Boc-FLFLF, Boc-phenyl-D-leucyl-phenyl-D-leucyl-phenylalanine; CCD, charge-coupled device; CLSM, confocal laser scanning microscopy; fMLP, *N*-formyl-methionyl-leucyl-phenylalanine; FRAP, fluorescence redistribution after photobleaching; GPCR, G protein-coupled receptor; HBS, HEPES-buffered solution; GRP1, general receptor for phosphoinositides-1; HEK, human embryonic kidney; PH, pleckstrin homology; PI(4,5)P_2, phosphatidylinositol-4,5-bisphosphate; PI(3,4,5)P_3, phosphatidylinositol-3,4,5-trisphosphate; PI3K, phosphoinositide 3-kinase; TIRFM, total internal reflection fluorescence microscopy; YFP, yellow fluorescent protein.

10.1021/bi800596b CCC: $40.75
Published on Web 10/02/2008

HEK293 cells overexpressing G$\beta\gamma$, a plasma membrane enrichment of GFP-tagged p101 or of the truncated $p101_{650-850}$ was detected by confocal laser scanning microscopy (CLSM) (*5, 10*). However, even though binding of p101 to the plasma membrane after release of G$\beta\gamma$ following GPCR activation was demonstrated by immunological assays (*11, 12*), a plasma membrane association of p101 or of its high-affinity G$\beta\gamma$-binding domain $p101_{650-850}$ was only detectable by imaging methods so far, when G$\beta\gamma$ was overexpressed but not after receptor stimulation (*5*).

To detect even small amounts of plasma membrane-associated biosensors with increased sensitivity compared to confocal laser scanning microscopy (CLSM), we applied total internal reflection fluorescence microscopy (TIRFM). TIRFM is the method of choice to selectively excite fluorescent molecules in the vicinity of the plasma membrane (*13*). With a penetration depth of 100−150 nm, evanescent wave excitation restricts the *z*-axis to a volume that is smaller than that of CLSM and most other fluorescence-based live cell imaging methods.

To further improve detection and quantification of weak plasma membrane association, we developed a mobility-based approach. Since diffusion depends on the Stokes radius of the diffusing particle and on the viscosity of the surrounding medium, changes in the localization and size of proteins lead to altered mobility which can be used as a read-out to follow signal transduction events. Most prominently, the diffusion coefficients of plasma membrane-associated and cytosolic proteins differ by more than 1 order of magnitude (*14*−*16*). Changes in the lateral mobility of translocating biosensors may, thus, be utilized to monitor signal transduction events with high sensitivity and in a time-resolved manner.

Fluorescence redistribution after photobleaching (FRAP), which was first described by Axelrod (*17*) has been widely employed to determine diffusion coefficients of fluorescent proteins (*15*). Here, we developed a microscopic device that enabled us to photobleach a diffraction-limited spot and to monitor the fluorescence redistribution using TIR illumination, in order to utilize the increased sensitivity of TIRFM to analyze processes near the plasma membrane. To follow translocation events from and to the plasma membrane, we applied repetitive FRAP measurements at the same location of the cell before and after stimulation. Here, we detected and quantified the GPCR-induced G$\beta\gamma$ release and, thus, established YFP-tagged $p101_{650-850}$ as a translocating G$\beta\gamma$ biosensor protein. This enabled us to evaluate the signal amplification between G$\beta\gamma$ release and $PI(3,4,5)P_3$ formation using the TIR/FRAP approach.

EXPERIMENTAL PROCEDURES

Generation of Expression Plasmids. YFP-$p101_{650-850}$ was generated by subcloning the sequence of $p101_{650-850}$ from the N-terminal fusion vector with CFP (*10*) into a custom-made N-terminal YFP fusion vector (*10*) using the restriction sites Hind III and Xba I. To clone the rat orthologue of $p87^{PIKAP}$, total RNA from whole hearts of 2-day-old Wistar rats was reverse-transcribed using oligo-dT primers and Superscript III reverse transcriptase (Invitrogen). The coding sequence was obtained by PCR with the primers 5′-TCC TTC CCT TAC AGG ACA GGC-3′ and 5′-GAC GCC CAG TGA GGC TGT C-3′ and subcloning into pcDNA3.1/V5/His-TOPO. Compared to an annotated sequence found in the ENSEMBL database (gene ENSRNOG00000003992, release 33) sequencing of several clones consistently yielded two point mutations. Because these mutations render the obtained sequence identical to the wild-type murine orthologue on both cDNA and protein level, it was concluded that the clones obtained have the correct sequence. The coding sequence was deposited in the DDBJ/EMBL/GenBank databases under accession number EF207569. To allow C-terminal fusion of rat $p87^{PIKAP}$ to a FLAG tag, a 3′ Xba I restriction site was introduced by PCR with the primers 5′-GCC ACC ATG GAG AGC TCA GAT GTG-3′ and 5′-TCT AGA TGG ATG ATG CCA GAG AAT GTG-3′. The PCR product was first subcloned into pcDNA3.1/V5/His-TOPO (Invitrogen) and then into a custom-made pcDNA3-FLAG (*18*) via Acc65 I and Xba I.

Cell Culture and Transfection. HEK293 cells (ATCC, Manassas, VA) were maintained in minimal essential medium with Earle's salts supplemented with 10% fetal calf serum, 100 g/mL streptomycin, and 100 U/mL penicillin (37 °C, 5% CO_2). Cells were seeded onto poly-L-lysine-coated glass coverslips in 35-mm cell culture dishes. Transfections with expression plasmids encoding YFP-fused membrane targeting domain of p101 (YFP-$p101_{650-850}$), YFP-GRP1(PH) (10), Gβ_1, Gγ_2, p101, p110γ, the fMLP receptor (*5*), and rat $p87^{PIKAP}$ were performed using a Fugene 6 transfection reagent (Roche Molecular Biochemicals, Mannheim, Germany) at a confluency of about 70% according to the manufacturer's instructions. To minimize preactivation of PI3K by serum-derived stimuli, HEK293 cells were maintained in serum-free medium for at least 24 h prior to experiments.

RBL-2H3 cells (ATCC, Manassas, VA) were maintained in minimal essential medium with Earle's salts supplemented with 10% fetal calf serum, 100 g/mL streptomycin, and 100 U/mL penicillin (37 °C, 5% CO_2).

Nucleofection of RBL-2H3 cells with YFP-$p101_{650-850}$ or YFP-GRP1(PH) was performed using the Nucleofector technology (Amaxa). A total of 5 μg DNA was diluted into 100 μL of the nucleofection solution (Cell Line Nucleofector Solution V), mixed with 6×10^6 cells, and nucleofected with program T-20. Cells were plated immediately onto 6 poly-L-lysine-coated glass coverslips in 35-mm cell culture dishes. After nucleofection, cells were grown in the presence of 10% serum for at least 16 h and maintained for additional 3−6 h in serum-free medium.

Confocal Fluorescence Imaging. All experiments were performed 18−48 h after transfection in HEPES-buffered solution (HBS), containing 10 mM HEPES (pH 7.4), 134 mM NaCl, 6 mM KCl, 1 mM $MgCl_2$, 1 mM $CaCl_2$, 5.5 mM glucose, and 0.2% (w/v) bovine serum albumin. Glass coverslips were mounted onto the stage of an inverted CLSM (LSM 510Meta, Carl Zeiss, Germany). Imaging of the YFP fusion proteins was carried out with the 488-nm line of an Ar^+ laser using a dichroic mirror (reflective below 488 nm) and a 530-nm long pass emission filter with an α-Plan Fluar 100×/1.45 objective (Zeiss).

TIRF Imaging and FRAP Measurements in TIRF Configuration. The setup for TIRF imaging in combination with spot photobleaching is schematically shown in Figure 1.

To excite YFP, the 488-nm line of an Ar^+ laser (Lasos, Germany) was selected by an acousto-optic tunable filter

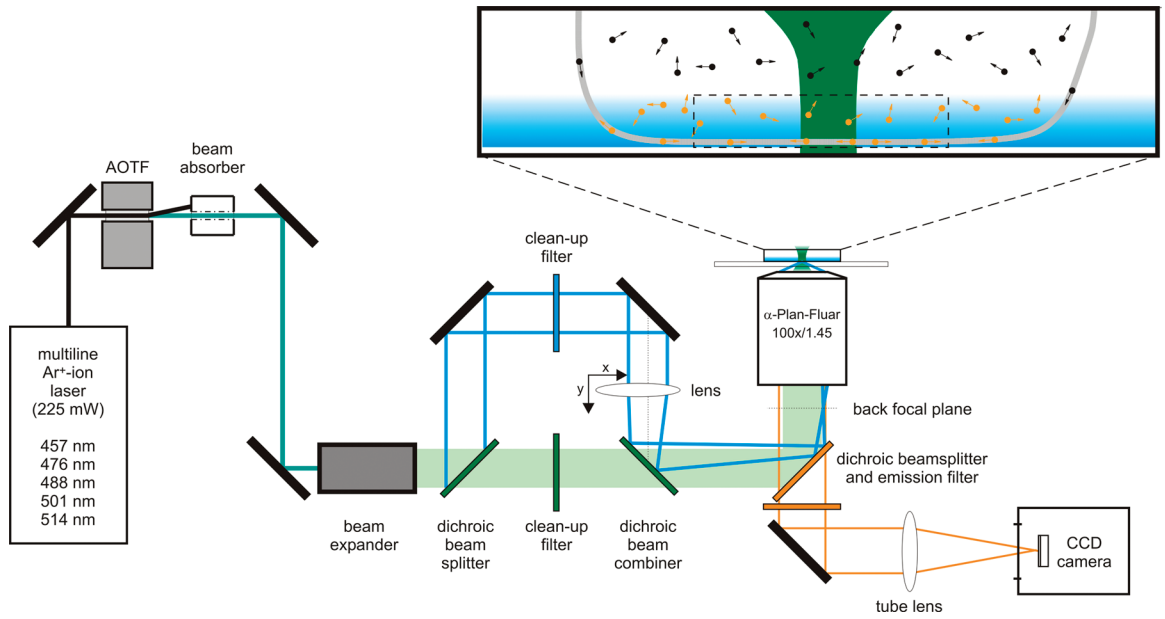

FIGURE 1: Beampath for TIRF imaging in combination with spot photobleaching. Excitation wavelengths from a multiline Ar^+ laser are selected by an AOTF. After 16× beam expansion, the 488-nm laser line (cyan) is coupled out by a dichroic mirror to pass an achromatic lens ($f = 250$ mm), which focuses the beam into the back-focal plane of the objective. Focusing is achieved by moving the lens in the *y*-direction. By moving the lens out of the optical axis (in the *x*-direction), TIR illumination is obtained. Another dichroic mirror is used to recombine the 488-nm beam with the unfocused 514-nm beam (green). The latter is used for spot photobleaching. The resulting illumination within an adherent cell is shown schematically in the inset. TIR illumination includes the plasma membrane (gray) and parts of the cytosol. Fluorescent molecules that are excited by TIR illumination are shown in orange; molecules outside this illumination volume are depicted in black. The volume bleached by the 514-nm line is shown in green. The volume, imaged in a typically FRAP experiment in TIRF configuration, is indicated by the dashed box.

(AOTF, AA Opto-Electronic, Orsay Cedex, France). The laser beam was expanded to about 16 mm and, for prismless total internal reflection (*19*), focused into a radial position on the back focal plane of an α-Plan Fluar 100×/1.45 objective (Zeiss). This was achieved by moving the focusing lens out of the optical axis, leading to a lateral displacement of the excitation beam (*20*). A 514-nm beamsplitter (Chroma, Rockingham, VT) was used to separate excitation and emission, and fluorescence light was detected through a 514-nm RazorEdge long pass filter (Semrock, Rochester, NY). Image acquisition was performed with a back-illuminated EM-CCD camera (iXon DV887, Andor, Belfast, UK) or in some initial experiments with a cooled CCD camera (Sensicam QE, PCO, Kelheim, Germany) using TillVision software (TILL Photonics, Gräfelfing, Germany).

For spot photobleaching, the 514-nm laser line was used. This allowed the separation of the beampath for TIRF imaging and spot photobleaching by two dichroic mirrors (505 nm, Chroma). The lens focusing the 488-nm beam into the back focal plane of the objective was, thus, bypassed, and the 514-nm bleaching beam was focused to a small spot by the objective. Switching between the lines and reduction of the power of the 488-nm laser line to avoid bleaching during image acquisition was realized using the AOTF on the microsecond time scale. Line separation of 488- and 514-nm beampaths was further improved by appropriate clean up filters (Chroma). Images of an area of interest (AOI) were recorded at low laser power using the 488-nm line in TIRF mode. Point bleaching was performed by focusing the 514-nm line at high laser power into a spot located in the center of the preselected AOI for 1−3 ms. A series of 16 prebleach images and 20 postbleach images was recorded. Up to 45 FRAP experiments were repeated in the same AOI every 5−20 s.

FRAP Data Analysis. For analysis of FRAP data from point-bleach measurements in TIRF configuration, we regard the first postbleach image as initial condition (*21*). The following recorded postbleach images (denoted simply as postbleach images here) are used to fit the mobility parameters. To this end, the intensity profile of the first postbleach image is convolved with the solution of the diffusion equation in two dimensions to simulate the intensity development over time for given diffusion coefficients. By minimizing the sum of squared residuals of this simulated intensity development and the measured postbleach images, the mobility parameters are determined. This allows for the extraction of diffusion coefficients without exact knowledge of the bleach geometry and timing.

Pixel intensities and timings of the TIRF measurements were extracted from a background-corrected 16-bit TIFF data file and a time code data file, respectively, generated by the acquisition software. Image pixel size was calculated from the magnification of the objective and the pixel size of the chip of the CCD camera. In 1× binning mode with the iXon DV887 and in 2× binning mode with the Sensicam QE, the pixel sizes of the images were 160 and 129 nm, respectively.

To account for inhomogeneities of the marker distribution, 16 images preceding the bleach event were recorded. Postbleach images were divided by the mean of prebleach images to obtain normalized intensities. In order to include the fluorescence intensities outside the recorded image which represent molecules that might diffuse into the recorded image area, the normalized bleach image was surrounded by pixels with an intensity of unity to calculate the convolution.

When all fluorescent molecules are assumed to diffuse with the same velocity, this is referred to as a one component model. Analysis of molecules with two distinct mobilities

was performed by superposing two diffusional processes with different diffusion coefficients and amplitudes. This is referred to as the two component model (*22*).

In case of one component analysis, the diffusion coefficients were determined by Brent's algorithm (*23*) by minimizing the χ^2 value. The value obtained at maximal cytoplasmic location of a protein served as the starting value for the fast diffusion coefficient D_2 in the two component analysis. Here, both diffusion coefficients were evaluated by Brent's algorithm, while for every iteration step of D_1, D_2 was optimized. The amplitudes corresponding to the diffusion coefficients were calculated by means of generalized linear least-squares regression using QR decomposition. The whole fitting algorithm was adapted from the variable projection approach (*24, 25*). To increase the robustness of data analysis, the individual diffusion coefficients of repetitive bleach experiments on one cell were linked and fitted globally, i.e., only two different diffusion coefficients were assumed to describe all bleach experiments, while the amplitudes were calculated individually for each photobleaching event.

We tested for an immobile fraction by assuming an additional component with an unchanged fluorescence distribution (i.e., that of the normalized first postbleach image) over time, whose amplitudes were determined by QR decomposition (see above). In our experimental data, the determined amplitudes of this fraction were negligible. Therefore, an immobile fraction was not considered for the proteins used in this study.

Algorithms were programmed in C using the GNU scientific library (*26*). The code is available on request from the authors.

RESULTS

Characterization of Plasma Membrane Association of Fluorescent Biosensors using CLSM. The membrane targeting domain of p101 has been previously mapped to the C-terminal amino acids 650−850 (*10*). Since this isolated domain exhibits a more efficient binding to G$\beta\gamma$ compared to the full-length subunit, we reasoned that a fluorescence-tagged version of this protein, YFP-p101$_{650-850}$, may yield a putative sensor for G$\beta\gamma$ release. HEK293 cells transfected with YFP-p101$_{650-850}$ in addition to Gβ_1 and Gγ_2 show a plasma membrane localization of the fluorescent biosensor (Figure 2A) (*10*). In contrast, the fluorescent biosensor for PI(3,4,5)P_3 was found exclusively in the cytosol in HEK293 cells overexpressing Gβ_1 and Gγ_2 (Figure 2A), because HEK293 cells do not express an endogenous PI3Kγ.

Upon stimulating HEK293 cells, which were transfected with the fMLP receptor and YFP-p101$_{650-850}$, with 1 μM fMLP, we failed to detect a translocation of YFP-p101$_{650-850}$ by CLSM (Figure 2B), indicating that the transient GPCR-mediated increase in cellular free G$\beta\gamma$ may be too small to resolve a plasma membrane enrichment of YFP-p101$_{650-850}$ using this method.

In HEK293 cells transiently coexpressing YFP-GRP1(PH), the fMLP receptor, and PI3Kγ subunits p101 and p110γ, stimulation with 1 μM fMLP evoked a marked increase in plasma membrane localization of the PI(3,4,5)P_3-binding PH domain (Figure 2C) (*5*). The previously observed slight basal membrane localization (*5*), which has been attributed to a constitutively active fMLP receptor by these authors, was

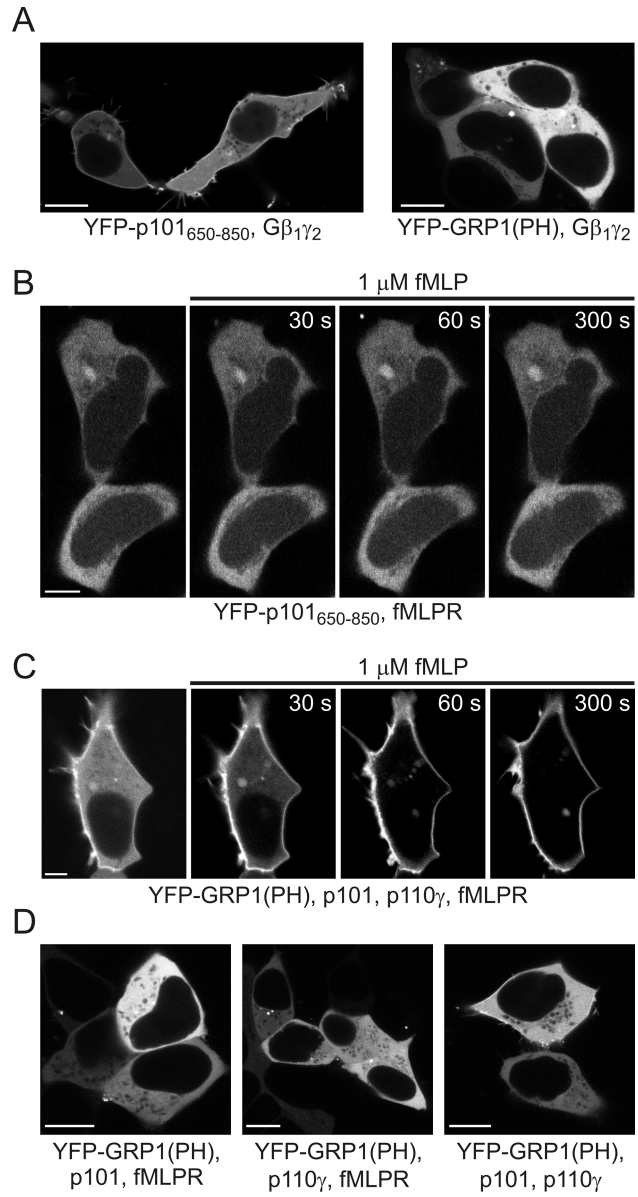

FIGURE 2: Confocal images of translocating fluorescent biosensors. (A) HEK293 cells overexpressing G$\beta\gamma$. YFP-p101$_{650-850}$ partially locates to the plasma membrane (left image), whereas overexpression of G$\beta\gamma$ does not lead to a plasma membrane location of YFP-GRP1(PH) in cells that do not express PI3Kγ (right image). (B) Fluorescence of HEK293 cells expressing YFP-p101$_{650-850}$ and the fMLP receptor monitored continuously using a CLSM before and after stimulation with 1 μM fMLP. The time points of image acquisition after addition of fMLP are indicated. (C) Translocation of YFP-GRP1(PH) to the plasma membrane in HEK293 cells additionally expressing the fMLP receptor; the regulatory p101 and the catalytic p110γ subunit of PI3Kγ before and after stimulation with 1 μM fMLP. The time points of image acquisition after addition of fMLP are indicated. (D) Localization of YFP-GRP1(PH), expressed in combination with PI3Kγ subunits and the fMLP receptor as indicated. Bars: 10 μm.

confirmed. To further investigate the origin of this basal membrane localization, we generated cells expressing the fluorescent biosensor and either of the PI3Kγ subunits in combination with the fMLP receptor or cells expressing both PI3Kγ subunits in the absence of the fMLP receptor (Figure 2D). When only either the catalytic or regulatory subunit of PI3Kγ and the fMLP receptor were present, no plasma membrane localization of YFP-GRP1(PH) was detected. In contrast, expression of both p101 and p110γ provoked a

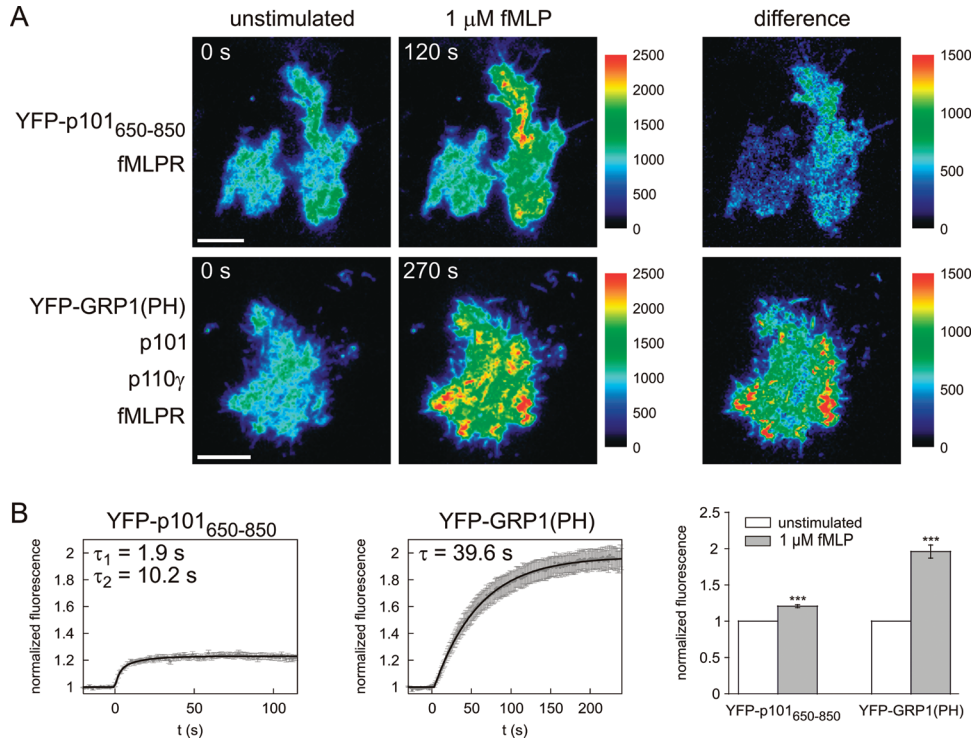

FIGURE 3: Translocation of autofluorescent biosensor proteins monitored using TIRF imaging in living cells. To monitor release of Gβγ or generation of $PI(3,4,5)P_3$ using translocating biosensors, HEK293 cells were transiently transfected with expression plasmids encoding either YFP-$p101_{650-850}$ and the fMLP receptor or with plasmids encoding YFP-GRP1(PH), the fMLP receptor, and PI3Kγ subunits p101 and p110γ. Translocation to the plasma membrane after stimulation with 1 μM fMLP at $t = 0$ s resulted in an increase in the YFP fluorescence intensity under TIR-illumination. TIRF images were acquired every second. (A) Fluorescence intensities before and after stimulation with fMLP shown as background-corrected pseudocolor images of one representative measurement. (right panels) Difference images obtained by subtracting the initial images from images acquired after fMLP stimulation. (B) Increase in fluorescence intensity quantified by calculating the mean fluorescence intensity from regions of interest at the location of cells using background-corrected images. (left panels) Time course of normalized fluorescence intensities averaged over 15−21 cells. (right panel) Quantification of intensities during stimulation with 1 μM fMLP. Statistical significance was tested using a paired *t*-test applied to non-normalized data ($p < 0.001$). Error bars indicate a standard error (SE) of 15−21 cells.

slight plasma membrane localization of the marker even in the absence of the fMLP receptor. However, this plasma membrane association was weaker than that found in the presence of the fMLP receptor. Moreover, Boc-FLFLF, an inhibitor of the fMLP receptor (*27*), partly reversed the basal plasma membrane localization of YFP-GRP1(PH) (Supporting Information Figure 1A). When the human histamine H4 receptor, another $G\alpha_i$-coupled receptor, was overexpressed, we observed a similar basal plasma membrane localization of YFP-GRP1(PH), which was partly reversible by addition of the inverse agonist thioperamide (Supporting Information Figure 1B). We conclude that basal plasma membrane localization of YFP-GRP1(PH) might orginate from a combination of Gβγ release caused by constitutively active fMLP receptor and, to a minor extent, from stimuli from the cell culture medium leading to a slight activation of other $G\alpha_i$-coupled receptors.

The clearly detectable plasma membrane translocation of the YFP-GRP1(PH) compared to that of the Gβγ sensor YFP-$p101_{650-850}$ points to the signal amplification between Gβγ production and the generation of $PI(3,4,5)P_3$ in the next step of the signal cascade.

TIRF-Based Detection of Plasma Membrane Association. Since the resolution of CLSM was not sufficient to detect a plasma membrane association of YFP-$p101_{650-850}$ upon fMLP-mediated Gβγ release, we applied TIRFM, which more sensitively reflects processes occurring at the plasma membrane. Indeed, an increase in YFP-$p101_{650-850}$ fluorescence was detectable in the TIRF configuration after stimulating fMLP receptor-expressing HEK293 cells with 1 μM fMLP (Figure 3). This plasma membrane translocation was rapid, with an initial half-time of about 2 s, which is close to the diffusion limit and a slower second phase with a half-time of about 10 s. As expected, the increase in fluorescence after stimulating HEK293 cells transiently expressing YFP-GRP1(PH), the fMLP receptor and PI3Kγ subunits p101 and p110γ with 1 μM fMLP was more pronounced (Figure 3). Remarkably, YFP-GRP1(PH) translocation followed a monoexponential kinetics and, showing a half-time of about 40 s, was much slower than that of YFP-$p101_{650-850}$ after fMLP addition. This kinetics may reflect the continuous activity of PI3Kγ after Gβγ-mediated activation. For both biosensors, we found a similar concentration response to the agonist with an EC_{50} of about 0.2 nM fMLP (data not shown).

Mobility-Based Quantification of Plasma Membrane Association. To further characterize the signal amplification between Gβγ release and $PI(3,4,5)P_3$ formation, we used a mobility-based approach. Since diffusion coefficients between plasma membrane-bound and cytosolic proteins differ by more than 1 order of magnitude (*14*−*16*), this parameter may be especially useful to detect even small changes in the localization of biosensors. To follow changes in the mobility of translocating biosensors, we designed a FRAP

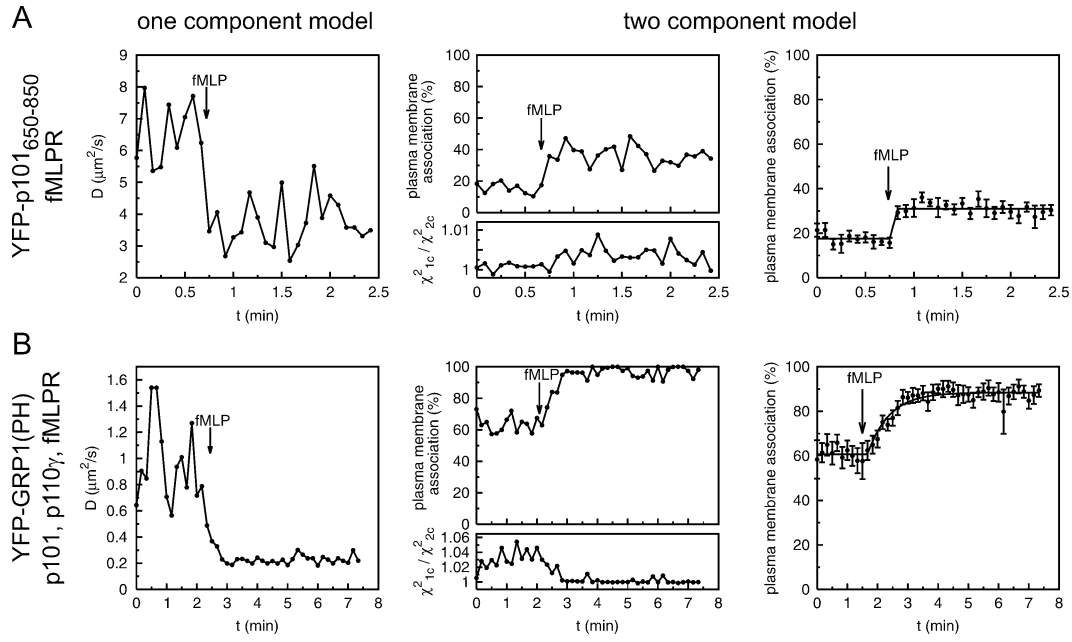

FIGURE 4: Analysis of translocation efficiency using repetitive FRAP analysis. Mobility of YFP-p101$_{650-850}$ (A) and YFP-GRP1(PH) (B) in HEK293 cells additionally expressing the fMLP receptor or the fMLP receptor and PI3Kγ subunits p101 and p110γ, respectively, was monitored by repetitive FRAP experiments. After 10 bleach cycles, cells were stimulated with 1 μM fMLP (indicated by arrows). Mean diffusion coefficients from analysis of one data set using the one component model are shown in the left panels for a representative measurement. The fraction of plasma membrane-associated biosensors was determined by analyzing the same data using the global two component model (middle panels). The lower middle panels show the ratio of χ^2 values obtained from the one component (1c) and two component (2c) models, which is highest when the one component model is least appropriate. The right panels show the mean plasma membrane association of the biosensors obtained from 6−12 independent measurements. Error bars indicate SE.

approach that allows continuous determination of diffusion coefficients in TIRF configuration. To this end, a setup that allows spot photobleaching in TIRF configuration was developed. Bleaching was repeatedly performed in the same region at the bottom of the cell while the agonist was applied. Furthermore, a novel, convolution-based method to analyze FRAP data using the whole image information was applied.

To compare the fMLP-induced translocation of YFP-p101$_{650-850}$ and YFP-GRP1(PH), HEK293 cells were transiently transfected with plasmids encoding YFP-p101$_{650-850}$ and the fMLP receptor or YFP-GRP1(PH), the fMLP receptor, p101, and p110γ. Repetitive FRAP experiments were performed, and after 10 bleach cycles, cells were activated with 1 μM fMLP, leading to a plasma membrane association of the biosensors YFP-p101$_{650-850}$ and YFP-GRP1(PH). Data were first analyzed using a one component model that determined one (mean) diffusion coefficient for each bleaching event. Translocation to the plasma membrane was associated with a decrease in this diffusion coefficient. However, it is reasonable to assume that the measured fluorescence redistribution profile is a superposition of two diffusion processes with a fast cytoplasmic and a slower plasma membrane-attached population of fluorescent proteins. To quantitatively assess the percentage of plasma membrane association within the imaged volume, we applied a global two component model for FRAP data analysis. Thus, for every cell analyzed by continuous photobleaching two diffusion coefficients of soluble and membrane-bound fluorescent biosensors were evaluated globally while their amplitudes were determined for every bleach event (Figure 4A and B). The application of the two component model was justified by a decrease of the calculated χ^2 values compared to the one component fit. As expected, the ratio of χ^2 values arising from the one versus two component model was highest, i.e. the one component model was least justified, when the amplitudes of the cytosolic and plasma membrane-bound fraction determined by the global two component model were about equal.

Plasma membrane translocation of YFP-p101$_{650-850}$ was clearly detectable by the mobility-based approach (Figure 4A). Remarkably, even in unstimulated cells about 17% of the biosensor within the TIR volume were plasma membrane-bound, indicating that minor amounts G$\beta\gamma$ are released by constitutively active fMLP receptor or other processes. Upon stimulation with 1 μM fMLP, this fraction increased to about 31% of the biosensor within the TIR volume. This increase was rapid, and the kinetics could not be resolved with the FRAP-technique (bleaching was repeated every 5 s). The mean diffusion coefficients and their standard errors determined from 6 independent measurements were 8.8 $\pm$ 1.2 and 0.28 $\pm$ 0.07 μm^2/s for the cytosolic and membrane-associated fractions, respectively.

To analyze the signal amplification, the PI(3,4,5)P$_3$-induced translocation of YFP-GRP1(PH) after fMLP stimulation was analyzed by the FRAP approach. Due to the basal G$\beta\gamma$ release, about 60% of YFP-GRP1(PH) within the TIR volume appeared already plasma membrane-bound before stimulation. This fraction increased to about 90% upon addition of 1 μM fMLP. The kinetics of this increase (half-time of about 30 s) is similar to that found for the increase in fluorescence intensity in TIRF configuration (see above). From 12 independent measurements, mean diffusion coefficients for the cytosolic and membrane-associated fractions were determined as 28.6 $\pm$ 4.8 and 0.20 $\pm$ 0.01 μm^2/s, respectively.

Quantification of Signal Amplification. For quantification of the signal amplification between G$\beta\gamma$ release and PI(3,4,5)P$_3$ formation, the plasma membrane enrichment of

Table 1: Enrichment of YFP-Tagged Proteins in the Plasma Membrane before and after Stimulation of HEK293 Cells with 1 μM fMLP, Calculated from the Repetitive TIR/FRAP Measurements Shown in Figure 4

	preactivation	postactivation
YFP-p101$_{650-850}$	3.5 ± 0.5	7.5 ± 0.7
YFP-GRP1(PH)	35.5 ± 1.7	189 ± 29

the respective fluorescent biosensor was evaluated before and after stimulating the cells with 1 μM fMLP. The excitation intensity of the evanescent field decreases exponentially with distance z from the glass−water interface according to

$$I(z) = I_0 \, e^{-z/d} \tag{1}$$

with

$$d = \frac{\lambda_0}{4\pi}(n_1^2 \sin^2 \theta - n_2^2)^{-1/2} \tag{2}$$

λ_0 denotes the used wavelength, θ the angle of incidence of the excitation beam, and n_1 and n_2 are the refractive indices of glass and the biological sample, respectively.

Assuming $n_1 = 1.52$ and $n_1 = 1.37$ in combination with an angle of incidence of 70°, the illumination profile for excitation using the 488-nm laser line can be calculated. Under this configuration, about 5.5% of the excitation light intensity would cross membrane-bound and 94.5% cytosolic biosensors, assuming that the first 5 nm above the membrane are occupied by plasma membrane-associated proteins. Knowing the distribution of excitation intensity within the TIR volume, one can estimate the enrichment of biosensors in the plasma membrane compared to the same volume in the cytosol from the amplitude coefficients calculated from the two component FRAP model (see above). These amplitude coefficients a are proportional to the number of excited molecules residing in either of the compartments. Therefore, the enrichment factor of a protein at the plasma membrane f_{PM} is given by

$$f_{PM} = \frac{a_{PM}}{I_{PM}} \frac{I_C}{a_C} \tag{3}$$

where the indices PM and C denote plasma membrane-bound and cytosolic fractions, respectively. The excitation intensities I represent the fraction of the evanescent wave energy within each compartment, i.e. 5.5% for plasma membrane-associated and 94.5% for cytosolic parts of the cell, so that the calculated enrichment f_{PM} amounts to the factor by which the concentration of the plasma membrane-associated proteins differs from cytosolic ones.

Under these assumptions, the concentration of YFP-p101$_{650-850}$ associated with the plasma membrane in resting cells is about 3.5-fold higher than that within the cytoplasm. Upon fMLP-mediated G$\beta\gamma$ release, the plasma membrane-associated fraction increases to about 7.5-fold in the membrane over the same volume in the cytosol. YFP-GRP1(PH) is about 35 times enriched in the plasma membrane in resting cells and about 190 times after stimulation with fMLP (see Table 1). Thus, the estimated signal amplification between G$\beta\gamma$ release and PI(3,4,5)P$_3$ formation is about 25-fold.

To compare the quantitative data obtained by our TIR/FRAP measurements with the measurements of intensity increase under TIRF illumination caused by the translocation of fluorescent proteins to the plasma membrane, we calculated the theoretical signal intensity increase in TIRFM that would be expected from the plasma membrane enrichment calculated above from the amplitude coefficients of the FRAP data analysis. For this, we assumed that the volume occupied by plasma membrane-associated proteins is about 1% of that of the cytosol (estimating the cytoplasmic volume to 1−2 pL and the cell surface to 1500−2000 μm^2 with membrane-bound proteins in a range of 5−10 nm at the inner membrane leaflet). The sum of plasma membrane-bound and cytosolic proteins is constant before and after activation. Thus, the fraction of all cytosolic YFP-tagged proteins in a cell n_C is given by

$$n_C = \frac{1}{0.01 f_{PM} + 1} \tag{4}$$

and that of plasma membrane-bound fluorescent proteins n_{PM} by

$$n_{PM} = 1 - n_C \tag{5}$$

Because the volume that is occupied by cytosolic and plasma membrane-associated proteins is not changed during the experiment, the fraction of proteins in the cytosol n_C is proportional to the cytosolic concentration. The measured fluorescence intensity I^{Fl} before and after stimulation is, thus, given by

$$I^{Fl} \propto n_C I_C + n_C f_{PM} I_{PM} \tag{6}$$

with a changing value of f_{PM} and, thus, n_C.

Accordingly, the estimated intensity increase caused by YFP-GRP1(PH) translocation to the plasma membrane after fMLP stimulation is 1.8-fold, which is in very good agreement to the TIRF measurements (see Figure 3). For the translocation of YFP-p101$_{650-850}$ to the plasma membrane, the expected intensity increase from the FRAP measurements is about 1.15-fold which is similar to the amplitude corresponding to the fast phase of YFP-p101$_{650-850}$ translocation deduced from the intensity measurements (Figure 3).

Translocation of Fluorescent Biosensors and Signal Amplification in RBL-2H3 Cells. Since HEK293 cells do not express an endogenous PI3Kγ, measurements in these cells may be prone to artifacts caused by overexpression of PI3Kγ or of the fMLP receptor. Therefore, we transfected cDNA encoding YFP-p101$_{650-850}$ or YFP-GRP1(PH) into RBL-2H3 cells, which possess an endogenous PI3Kγ (Voigt, P., Schaefer, M., unpublished observation). G$\beta\gamma$ release was induced by stimulating the endogenous adenosine A3 receptor (*28*) with 10 μM IB-MECA.

In agreement with our confocal measurements using HEK293 cells, no translocation of YFP-p101$_{650-850}$ following stimulation of a Gα_i-coupled receptor was detectable in RBL-2H3 cells using CLSM (data not shown). Like in HEK293 cells, a slight basal plasma membrane enrichment of YFP-GRP1(PH) was observed by confocal imaging indicating basal activity of class I$_A$ or I$_B$ PI3 kinases. A slight increase in plasma membrane-associated YFP-GRP1(PH) after stimulation with 10 μM IB-MECA was detectable using CLSM (Figure 5A). However, this translocation was much less pronounced than that found after fMLP stimulation of HEK293 cells expressing PI3Kγ and fMLP receptor.

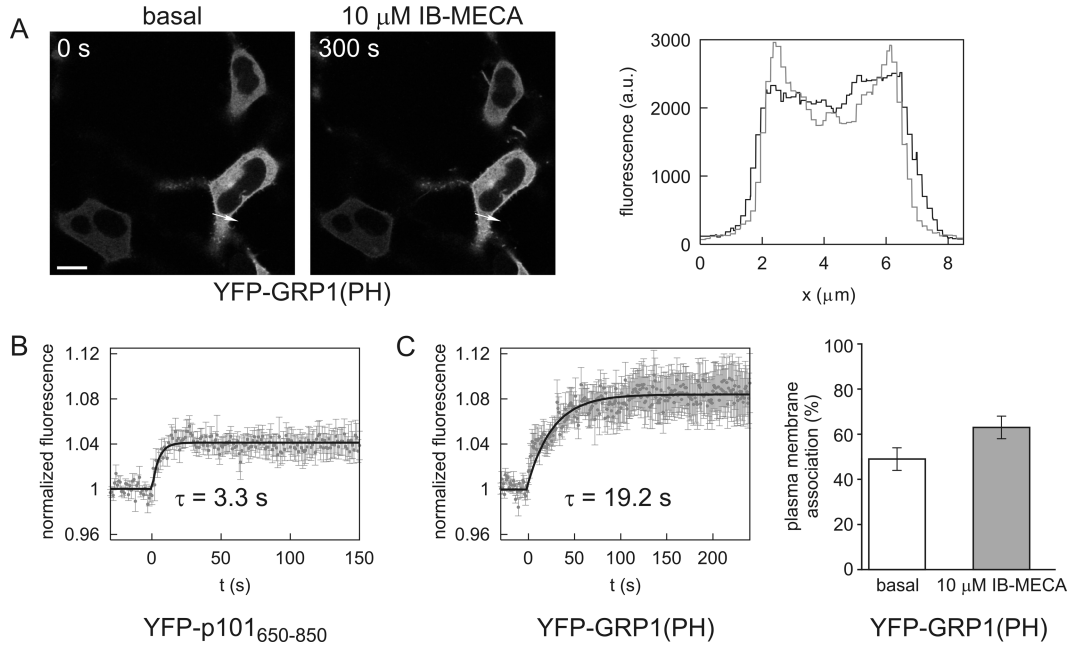

FIGURE 5: Translocation of fluorescent biosensors in RBL-2H3 cells. (A) Subcellular localization of YFP-GRP1(PH) in RBL-2H3 cells before and 300 s after stimulation with 10 μM IB-MECA was monitored by CLSM. Bar: 10 μm. The intensity profile along the indicated arrow is shown in the right panel. The gray line represents the profile before and the black line 300 s after stimulation. (B) Translocation of YFP-p101$_{650-850}$ after stimulation with 10 μM IB-MECA at $t = 0$ s detected by an increase in mean YFP fluorescence intensity under TIR illumination. Data represent means ± SE of measurements in 14 RBL-2H3 cells. (C) Translocation of YFP-GRP1(PH) in RBL-2H3 cells after addition of 10 μM IB-MECA at $t = 0$ s detected by an increase in YFP fluorescence under TIR-illumination (left panel). Data represent means ± SE of measurements in 9 cells. The right panel shows the amount of plasma membrane-associated YFP-GRP1(PH) within the TIR-illuminated volume before and after stimulation of RBL-2H3 cells with 10 μM IB-MECA deduced from a mobility-based approach. Data represent weighted mean ± SE of 20 measurements from 2 independent cells.

When the fluorescence intensity of RBL-2H3 cells was monitored under TIR illumination, the translocation of YFP-p101$_{650-850}$ to the plasma membrane after G$\beta\gamma$ release caused by stimulation with 10 μM IB-MECA was detectable by a very slight intensity increase (Figure 5B). This fluorescence intensity increase was lower than that observed after G$\beta\gamma$ release in fMLP-stimulated HEK293 cells that overexpressed the fMLP receptor. YFP-p101$_{650-850}$ translocation in RBL cells was monoexponential with a half-time of about 3 s. The translocation of YFP-GRP1(PH) to the plasma membrane after stimulating a Gα_i-coupled receptor was also followed by an intensity increase under TIR illumination (Figure 5C). The observed fluorescence intensity increase was much lower than that found in fMLP-stimulated HEK293 cells. In RBL-2H3 cells, YFP-GRP1(PH) translocation occurred with a half-time of about 20 s, which was slightly faster than that found in HEK293 cells.

Because the changes in the amount of plasma membrane-bound YFP-p101$_{650-850}$ in RBL-2H3 cells were so low, the expected increase in the amplitude corresponding to the slow fraction was lower than the uncertainty of the determination of amplitude coefficients from the TIR/FRAP analysis. For this reason, we were not able to detect significant changes in the mobility of YFP-p101$_{650-850}$ after stimulation of RBL-2H3 cells with 10 μM IB-MECA (data not shown). Plasma membrane association of YFP-GRP1(PH) in IB-MECA-stimulated RBL-2H3 cells could be followed by a decreased mobility and, thus, an increased plasma membrane-bound fraction using the TIR/FRAP approach in some of the investigated cells (Figure 5D).

To quantify the signal amplification between G$\beta\gamma$ release and PI(3,4,5)P$_3$ formation in RBL-2H3 cells, we calculated the putative membrane enrichment of YFP-p101$_{650-850}$ before stimulation from data of TIR/FRAP analysis, which revealed that about 13.3% of the YFP-p101$_{650-850}$ in the TIRF volume was plasma membrane-bound. According to eq 3, this corresponds to a plasma membrane enrichment of about 2.7-fold. The putative increase in plasma membrane association was then calculated from the intensity increase measured under TIR illumination using eqs 4−6 yielding a plasma membrane enrichment of about 3.7-fold after stimulation (Table 2). Formation of PI(3,4,5)P$_3$ measured by YFP-GRP1(PH) translocation was analyzed in the same way. The initial about 17-fold enrichment of YFP-GRP1(PH) in the plasma membrane of RBL-2H3 cells increased to about 21-fold according to the intensity-based measurements (Table 2). Because translocation of YFP-GRP1(PH) could be followed by TIR/FRAP measurements, the membrane enrichment of YFP-GRP1(PH) after stimulation can be directly calculated from the amplitude coefficients obtained by FRAP data analysis (Table 2). Notably, the plasma membrane enrichment after stimulation estimated via this approach is much higher than that calculated from the intensity measurements. An increase in the plasma membrane association was not detectable in all cells using the mobility-based approach,

Table 2: Enrichment of YFP-Tagged Proteins in the Plasma Membrane before and after Stimulation of RBL-2H3 Cells with 10 μM MIB-MECA, Calculated from Intensity Increase under TIRF Illumination and from the Repetitive TIR/FRAP Measurements Shown in Figure 5

	calculated from	preactivation	postactivation
YFP-p101$_{650-850}$	TIR/FRAP/TIRF-intensity	2.7 ± 0.5	3.7 ± 0.9
YFP-GRP1(PH)	TIR/FRAP/TIRF-intensity	16.7 ± 0.9	20.9 ± 1.3
YFP-GRP1(PH)	TIR/FRAP	16.7 ± 0.9	31.8 ± 1.3

and we only included cells that showed a decreased mobility after activation into the analysis. Thus, the plasma membrane-bound fraction after stimulation with IB-MECA might be overestimated using the TIR/FRAP analysis, explaining the discrepancy to the calculated values of plasma membrane-enrichment from the intensity measurements. From the values of YFP-p101$_{650-850}$ and YFP-GRP1(PH) enrichment at the plasma membrane after stimulation with 10 μM IB-MECA, we estimate a signal amplification of 5−10-fold between G$\beta\gamma$ release and PI(3,4,5)P_3 formation in RBL-2H3 cells.

The lower translocation of YFP-GRP1(PH) in RBL-2H3 cells compared to HEK293 cells transiently transfected with p101, p110γ, and the fMLP receptor might be explained by the different nature of the regulatory PI3Kγ subunit, since RBL-2H3 cells exclusively express the more recently identified p87^{PIKAP} regulatory subunit (Voigt, P., Schaefer, M., unpublished observation). To test this hypothesis, we transfected HEK293 cells with expression plasmids encoding p87^{PIKAP}, p110γ, and the fMLP receptor and monitored the translocation of YFP-GRP1(PH) by confocal imaging or using TIR-illumination by an increase in the YFP fluorescence intensity and with the mobilty-based approach (Figure 6). Indeed, the amount of plasma membrane translocation in these cells was markedly reduced compared to cells expressing the p101 regulatory subunit. The plasma membrane translocation efficiency of YFP-GRP1(PH) in HEK293 cells expressing the p87^{PIKAP} regulatory subunit was similar to that found in RBL-2H3 cells. From the two component FRAP analysis, we calculate the plasma membrane enrichment to about 8-fold before and about 19-fold after stimulation with 1 μM fMLP. The signal amplification between G$\beta\gamma$ release and PI(3,4,5)P_3 formation is, thus, only about 2.5-fold in HEK293 cells expressing the p87^{PIKAP} adapter protein.

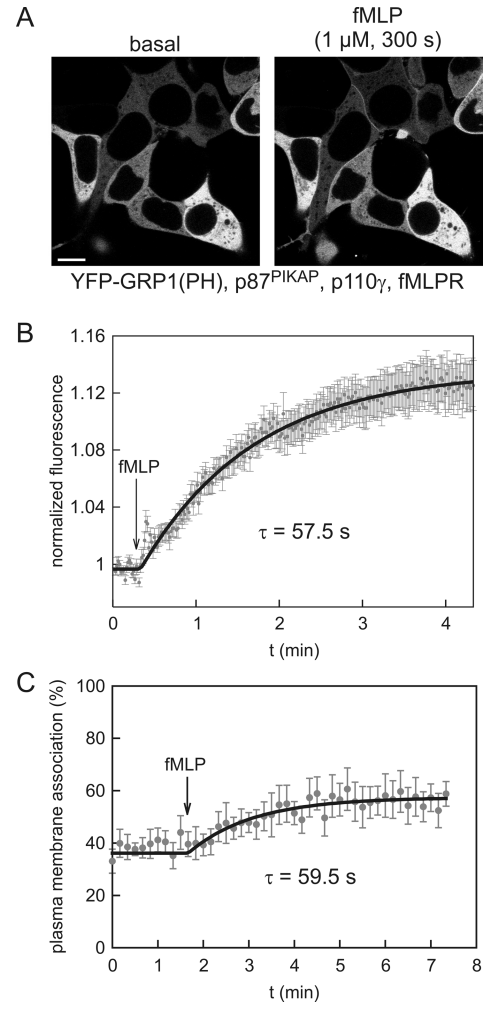

FIGURE 6: Translocation of YFP-GRP1(PH) in HEK293 cells with the p87^{PIKAP} regulatory subunit. (A) Translocation of YFP-GRP1(PH) in HEK293 cells transiently transfected with p87^{PIKAP}, p110γ, and the fMLP receptor induced by the addition of 1 μM fMLP at $t = 0$ s monitored by CLSM. (B) Translocation of YFP-GRP1(PH) after addition of 1 μM fMLP at the time point indicated by an arrow detected by an increase in mean YFP fluorescence intensities under TIR illumination. Data represent means ± SE of measurements in 29 HEK293 cells. (C) Amount of plasma membrane-bound YFP-GRP1(PH) within the TIR-volume before and after stimulation with 1 μM fMLP (arrow) quantified using the FRAP-based approach in combination with two component data analysis. Data represent mean ± SE of five independent measurements.

DISCUSSION

In this study we analyzed the Gα_i-coupled receptor-stimulated release of G$\beta\gamma$ and the signal amplification by the subsequent PI3Kγ-mediated production of PI(3,4,5)P_3 using translocating fluorescent biosensors.

In contrast to the regulatory subunit p85 of class I_A PI3Ks, which exhibits a plasma membrane translocation after receptor stimulation that is detectable by classical imaging approaches (*29*), the receptor-induced plasma membrane association of the PI3Kγ regulatory subunit p101 has not been observed by fluorescence microscopical techniques so far. Since under TIR illumination the plasma membrane at the bottom of the cell and only small parts of the cytoplasm above are excited, this technique is especially suitable to study translocation events to and from the plasma membrane (*30*). In contrast to CLSM, in TIRFM only the imaged area is illuminated by the laser beam, leading to low photoinduced damage of the imaged cells and to reduced photobleaching during image acquisition. By employing TIRFM, the translocation of YFP-p101$_{650-850}$ after transient stimulation of a Gα_i-coupled receptor could be clearly detected. Nevertheless, intensity-based TIRF measurements, which show an increase in fluorescence when the investigated protein binds to the plasma membrane, may suffer from artifacts caused by continuous photobleaching due to laser illumination. Moreover, quantification of the amount of translocating protein is not supported by this method. To develop a measure for the quantification of translocation efficiency, we extended the TIRFM approach to allow the detection of changes in protein mobility using FRAP. To combine TIR illumination with the ability to selectively point bleach a diffraction-limited region, we developed a setup where the different laser lines are used in two distinct beampaths: one serving for TIRF illumination and the other for focused point bleaching. By applying repeated bleaching at the same location and subsequent TIRF imaging of the cell, we were able to detect changes in cytoplasmic and membrane-associated pools of YFP-p101$_{650-850}$ in HEK293 cells. For data analysis, a convolution-based method was developed. To quantify the amount of plasma membrane association, we established a global two component model, which enables a robust FRAP evaluation directly yielding the fraction of membrane-bound and cytosolic proteins for each time point of repetitive measurements within one cell.

The generation of $PI(3,4,5)P_3$ by PI3Kγ, which represents the next step in the signaling cascade, can be easily followed by classical imaging techniques using YFP-GRP1(PH) as a translocating biosensor (*3, 5*). The remarkable amount of plasma membrane-bound YFP-GRP1(PH) that is present in resting PI3Kγ-transfected HEK293 cells may be due to PI3Kγ activation, which occurs to a small extent in an fMLP receptor-independent manner. Since neither of the subunits alone leads to a visible plasma membrane association of YFP-GRP1(PH), we suppose that a minor amount of G$\beta\gamma$ released by other stimuli activates PI3Kγ. Similar effects might be responsible for the basal plasma membrane enrichment of YFP-GRP1(PH) in RBL-2H3 cells. In addition, the overexpressed fMLP receptor itself exhibits a constitutive activity in HEK293 cells (*5*). In agreement, using the mobility-based approach, YFP-$p101_{650-850}$ was also found partly plasma membrane-associated in unstimulated cells. In addition, the basal enrichment of YFP-$p101_{650-850}$ at the plasma membrane might be caused partly by the biosensor itself, which acts as a scavenger for G$\beta\gamma$ and may thus prevent reassociation of G$\beta\gamma$ with Gα subunits. Taking into account that the volume occupied by plasma membrane-bound proteins is only about 1% of that of the cytosol, this basal plasma membrane enrichment is in fact quite low and is only detectable due to the strong accentuation of the plasma membrane-associated fluorescence in TIRFM.

Even though the mobility-based approach allows for a reliable detection of very small changes in plasma membrane association like that of p101 in HEK293 cells upon stimulation, it is afflicted by deviations in the amplitude coefficient determination of about 5%. Changes in the plasma membrane concentration of YFP-$p101_{650-850}$ in IB-MECA-stimulated RBL-2H3 cells are extremely small and would cause an increase in the amplitude of plasma membrane-bound proteins of less than 5%. Hence, we were unable to use the mobility-based approach for reliably determining the concentration of plasma membrane-bound biosensors after activation in RBL-2H3 cells. Nonetheless, the plasma membrane enrichment of YFP-$p101_{650-850}$ in RBL-2H3 cells can be quantified by calculating the membrane association in resting cells using the TIR/FRAP approach and its increase by monitoring the fluorescence increase under TIR illumination.

The signal amplification between G$\beta\gamma$ release and $PI(3,4,5)P_3$ generation was estimated to be about 25-fold in HEK293 cells overexpressing p101 and p110γ and about 5−10-fold in RBL-2H3 cells. This prediction presumes that the stoichiometry of binding of YFP-$p101_{650-850}$ to G$\beta\gamma$ is 1:1 like that for the binding of YFP-GRP1(PH) to $PI(3,4,5)P_3$ (*31, 32*). The lower signal amplification in RBL-2H3 cells is most likely caused by the different nature of the regulatory PI3Kγ subunit, since HEK293 cells expressing the $p87^{PIKAP}$ regulatory subunit in combination with p110γ show a similar low signal amplification. This result is in good agreement with previous observations showing that the $p87^{PIKAP}$ regulatory subunit binds G$\beta\gamma$ with a lower affinity compared to p101 (*8, 9*). The lower signal amplification in RBL-2H3 cells and in HEK293 cells expressing $p87^{PIKAP}$ compared to HEK293 cells expressing p101 may, thus, be attributed to a decreased adaptor activity of $p87^{PIKAP}$ compared to p101. Thus, the activation of PI3Kγ upon G$\beta\gamma$ release is decreased in cells expressing $p87^{PIKAP}$ compared to the p101 regulatory subunit.

Some approaches use a shift in the concentration response curve caused by a substrate depletion to determine signal amplification, an effect that is well recognized to underline the phenomenon of spare receptors. If the substrate conversion is not limiting, however, an amplification would result in higher amplitudes at constant EC_{50}. Since binding of PI3Kγ to G$\beta\gamma$ is assumed to occur in a 1:1 stoichiometry, signal amplification is merely given by the continuous catalytic activity of the membrane-recruited lipid kinase, which is also reflected by the slower kinetics of the YFP-GRP1(PH) translocation compared to that of the G$\beta\gamma$ sensor YFP-$p101_{650-850}$. It has been estimated that the resting and peak levels of $PI(3,4,5)P_3$ amount 0.01% and 1% of total $PI(4,5)P_2$ content in the cytoplasmic leaflet, respectively (*33*). Thus, the $PI(4,5)P_2$ pool does not significantly limit the signal amplitude, which is in agreement with a similar concentration dependence of the biosensors for G$\beta\gamma$ and $PI(3,4,5)P_3$ used in this study. It is still possible that saturation occurs in single cells at the level of $PI(3,4,5)P_3$ detection by a limited number of translocating biosensor proteins. Thus, due to a possible underestimation of $PI(3,4,5)P_3$ formation, the determined signal amplification in p101/p110γ expressing HEK293 cells may be higher than estimated here. In RBL-2H3 cells or in HEK293 cells expressing the $p87^{PIKAP}$/p110γ PI3Kγ isoform, saturation of the YFP-GRP1(PH) translocation was not observed, rendering the quantitative estimate somewhat more reliable, for the endogenous signaling cascade in RBL-2H3 cells or for the lower processivity of $p87^{PIKAP}$-complexed PI3Kγ.

The kinetics of YFP-$p101_{650-850}$ binding to the plasma membrane in HEK293 cells was faster than the resolution of our FRAP-based approach and, in fact, close to the diffusion limit (*34*). Notably, in addition to an initial fast translocation with a half-time of about 2 s, a second slower phase of YFP-$p101_{650-850}$ translocation with a half-time of about 10 s was resolved by measuring the intensity increase under TIR illumination. This second phase might be attributed to G-protein subunits that were redistributed to the plasma membrane from endomembranes (*35, 36*) during the course of the measurement. Remarkably, in RBL-2H3 cells YFP-$p101_{650-850}$ translocation was monoexponential with a half-time of about 3 s, suggesting that shuttling of G$\beta\gamma$ between plasma membrane and endomembranes might be less pronounced in these cells. In contrast to YFP-$p101_{650-850}$, YFP-GRP1(PH) associated much slower with the plasma membrane after fMLP stimulation. The half-time of about 30−40 s in HEK293 cells and 20 s in RBL-2H3 cells, thus, most likely corresponds to that of the production of $PI(3,4,5)P_3$ by PI3Kγ.

The diffusion coefficients of cytosolic and membrane-bound fractions of YFP-labeled proteins obtained by our method are in a similar range as those reported for other fluorescent proteins (*16, 37, 38*). For the cytosolic fractions, the diffusion coefficient is at the lower end of reported values for cytoplasmic proteins, which is in agreement with a slightly increased viscosity of the cytoplasm near the plasma membrane (*39*). The mobility of the plasma membrane-associated biosensors (0.2−0.3 $\mu m^2/s$) is somewhat lower than that reported for lipids (1 $\mu m^2/s$) (*40*). This is in agreement with the binding of YFP-GRP1(PH) to lipids or YFP-$p101_{650-850}$ to proteins that are membrane-bound by a lipid modification. The slower lateral movement may be

caused by the increased Stokes radius of the bound protein compared to a plasma membrane-lipid. In addition, phosphoinositides acting as membrane anchors for PH domains are reported to form poorly mobile clusters in some cells (*41, 42*), which may be the reason for slower apparent diffusion coefficients.

To our knowledge, detection of the transient release of endogenous G$\beta\gamma$ was not possible using an optical biosensor so far. Previous approaches utilized fluorescent tagged Gα and Gβ-versions in Gβ null mutant cells and detected G$\beta\gamma$ release by a decrease in FRET efficiency (*43*). To detect changes in free endogenous G$\beta\gamma$ using imaging approaches, the next amplification step within the signaling cascade, e.g. the generation of PI(3,4,5)P_3, had to be utilized which can be followed by fluorescent biosensors like YFP-GRP1(PH) (*3*). Here, we have shown that YFP-p101$_{650-850}$ can serve as an optical biosensor to directly monitor endogenous G$\beta\gamma$ release using TIRFM. Using TIRFM in combination with the detection of changes in the mobility of the biosensor, a quantification of G$\beta\gamma$ release is possible.

In conclusion, we developed a new tool to detect and analyze small changes in plasma membrane association that were not detectable by classical imaging methods so far. A large number of signal transduction mechanisms utilizes translocation of effector proteins. Repetitive FRAP analysis is, thus, suitable for monitoring a variety of processes that involve changes in the plasma membrane concentration of optical biosensors. Mechanisms leading to an association of proteins with the plasma membrane include posttranslational covalent lipid modification as it occurs at the CAAX motif (*44*), interaction of PH domains with phosphatidylinositol lipids (*45*), diacyl glycerol binding of C1 (*46*), or phosphatidylserine and Ca^{2+} binding of C2 domains (*47*), among others. In addition, binding of effector proteins to transmembrane receptors is a common principle in signal transduction. Prominent examples are proteins bearing Src homology 2 domains that can bind to certain phosphotyrosine motifs, e.g. at activated receptor tyrosine kinases (*48*). Changes in the membrane association of proteins can, thus, be mediated, e.g., by an altered lipid composition, an altered phosphorylation state of transmembrane receptors, or changes in intracellular calcium concentration. In spite of the relatively low temporal resolution of the FRAP approach, most dynamic processes in living cells can be unraveled and quantified by this technique. The convolution-based FRAP method may also be adapted to standard confocal laser scanning microscopes or to an epifluorescence microscope if equipped with an appropriate laser and a sensitive video-rate CCD. Likewise, the method is scalable to automated high content analysis and applicable to a wide range of already existing or specifically designed translocating fluorescent biosensors. We therefore conclude that convolution-based two component FRAP analysis provides a useful and sensitive tool for assaying a large number of signal transduction events in living cells by means of mobility-based translocation.

ACKNOWLEDGMENT

We thank Jürgen Malkewitz and Nadine Albrecht for excellent technical assistance.

SUPPORTING INFORMATION AVAILABLE

Reversal of the basal activity of the fMLP receptor or histamine H4 receptor by the antagonists Boc-FLFLF and thioperamide, respectively. This material is available free of charge via the Internet at http://pubs.acs.org.

REFERENCES

1. Vanhaesebroeck, B., Leevers, S. J., Ahmadi, K., Timms, J., Katso, R., Driscoll, P. C., Woscholski, R., Parker, P. J., and Waterfield, M. D. (2001) Synthesis and function of 3-phosphorylated inositol lipids. *Annu. Rev. Biochem. 70*, 535–602.
2. Cantley, L. C. (2002) The phosphoinositide 3-kinase pathway. *Science 296*, 1655–1657.
3. Gray, A., Van Der Kaay, J., and Downes, C. P. (1999) The pleckstrin homology domains of protein kinase B and GRP1 (general receptor for phosphoinositides-1) are sensitive and selective probes for the cellular detection of phosphatidylinositol 3,4-bisphosphate and/or phosphatidylinositol 3,4,5-trisphosphate in vivo. *Biochem. J. 344*, 929–936.
4. Guillou, H., Lecureuil, C., Anderson, K. E., Suire, S., Ferguson, G. J., Ellson, C. D., Gray, A., Divecha, N., Hawkins, P. T., and Stephens, L. R. (2007) Use of the GRP1 PH domain as a tool to measure the relative levels of PtdIns(3,4,5)P3 through a protein-lipid overlay approach. *J. Lipid Res. 48*, 726–732.
5. Brock, C., Schaefer, M., Reusch, H. P., Czupalla, C., Michalke, M., Spicher, K., Schultz, G., and Nürnberg, B. (2003) Roles of G$\beta\gamma$ in membrane recruitment and activation of p110γ/p101 phosphoinositide 3-kinase γ. *J. Cell Biol. 160*, 89–99.
6. Hawkins, P. T., and Stephens, L. R. (2007) PI3Kγ is a key regulator of inflammatory responses and cardiovascular homeostasis. *Science 318*, 64–66.
7. Stephens, L. R., Eguinoa, A., Erdjument-Bromage, H., Lui, M., Cooke, F., Coadwell, J., Smrcka, A. S., Thelen, M., Cadwallader, K., Tempst, P., and Hawkins, P. T. (1997) The G$\beta\gamma$ sensitivity of a PI3K is dependent upon a tightly associated adaptor, p101. *Cell 89*, 105–114.
8. Suire, S., Coadwell, J., Ferguson, G. J., Davidson, K., Hawkins, P., and Stephens, L. (2005) p84, a new G$\beta\gamma$-activated regulatory subunit of the type ib phosphoinositide 3-kinase p110γ. *Curr. Biol. 15*, 566–570.
9. Voigt, P., Dorner, M. B., and Schaefer, M. (2006) Characterization of p87^{PIKAP}, a novel regulatory subunit of phosphoinositide 3-kinase γ that is highly expressed in heart and interacts with PDE3B. *J. Biol. Chem. 281*, 9977–9986.
10. Voigt, P., Brock, C., Nürnberg, B., and Schaefer, M. (2005) Assigning functional domains within the p101 regulatory subunit of phosphoinositide 3-kinase γ. *J. Biol. Chem. 280*, 5121–5127.
11. Al-Aoukaty, A., Rolstad, B., and Maghazachi, A. A. (1999) Recruitment of pleckstrin and phosphoinositide 3-kinase γ into the cell membranes, and their association with G$\beta\gamma$ after activation of NK cells with chemokines. *J. Immunol. 162*, 3249–3255.
12. Naccache, P. H., Levasseur, S., Lachance, G., Chakravarti, S., Bourgoin, S. G., and McColl, S. R. (2000) Stimulation of human neutrophils by chemotactic factors is associated with the activation of phosphatidylinositol 3-kinase γ. *J. Biol. Chem. 275*, 23636–23641.
13. Axelrod, D. (1981) Cell-substrate contacts illuminated by total internal reflection fluorescence. *J. Cell Biol. 89*, 141–145.
14. Teruel, M. N., and Meyer, T. (2000) Translocation and reversible localization of signaling proteins: a dynamic future for signal transduction. *Cell 103*, 181–184.
15. Reits, E. A. J., and Neefjes, J. J. (2001) From fixed to FRAP: measuring protein mobility and activity in living cells. *Nat. Cell Biol. 3*, E145−E147.
16. Klonis, N., Rug, M., Harper, I., Wickham, M., Cowman, A., and Tilley, L. (2002) Fluorescence photobleaching analysis for the study of cellular dynamics. *Eur. Biophys. J. 31*, 36–51.
17. Axelrod, D., Koppel, D. E., Schlessinger, J., Elson, E., and Webb, W. W. (1976) Mobility measurement by analysis of fluorescence recovery after photobleaching. *Biophys. J. 16*, 1055–1069.
18. Hellwig, N., Albrecht, N., Harteneck, C., Schultz, G., and Schaefer, M. (2005) Homo- and heteromeric assembly of TRPV channel subunits. *J. Cell. Sci. 118*, 917–928.
19. Axelrod, D. (2001) Selective imaging of surface fluorescence with very high aperture microscope objectives. *J. Biomed. Opt. 6*, 6–13.

20. Axelrod, D. (2003) Total internal reflection fluorescence microscopy in cell biology. *Methods Enzymol. 361*, 1–33.
21. Sniekers, Y. H., and van Donkelaar, C. C. (2005) Determining diffusion coefficients in inhomogenous tissues using fluorescence recovery after photobleaching. *Biophys. J. 89*, 1302–1307.
22. Gordon, G. W., Chazotte, B., Wang, X. F., and Herman, B. (1995) Analysis of simulated and experimental fluorescence recovery after photobleaching. Data for two diffusing components. *Biophys. J. 68*, 766–778.
23. Brent, R. P. (1973) *Algorithms for minimization without derivatives (Prentice-Hall series in automatic computation)*, Prentice-Hall, Englewood Cliffs, NJ.
24. Golub, G. H., and Pereyra, V. (1973) The differentiation of pseudo-inverses and nonlinear least squares problems whose variables separate. *SIAM J. Numer. Anal. 10*, 413–432.
25. Golub, G. H., and Pereyra, V. (2003) Separable nonlinear least squares: the variable projection method and its applications. *Inverse Problems 19*, R1−R26.
26. Galassi, M., Davies, J., Theiler, J., Gough, B., Jungman, G., Booth, M., and Rossi, F. *Gnu scientific library reference manual*, 2nd ed.
27. Stenfeldt, A.-L., Karlsson, J., Wenneras, C., Bylund, J., Fu, H., and Dahlgren, C. (2007) Cyclosporin H, Boc-MLF and Boc-FLFLF are antagonists that preferentially inhibit activity triggered through the formyl peptide receptor. *Inflammation 30*, 224–229.
28. Ramkumar, V., Stiles, G., Beaven, M., and Ali, H. (1993) The A3 adenosine receptor is the unique adenosine receptor which facilitates release of allergic mediators in mast cells. *J. Biol. Chem. 268*, 16887–16890.
29. Gillham, H., Golding, M. C., Pepperkok, R., and Gullick, W. J. (1999) Intracellular movement of green fluorescent protein-tagged phosphatidylinositol 3-kinase in response to growth factor receptor signaling. *J. Cell Biol. 146*, 869–880.
30. Meyer, T., and Teruel, M. N. (2003) Fluorescence imaging of signaling networks. *Trends Cell Biol. 13*, 101–106.
31. Ferguson, K. M., Kavran, J. M., Sankaran, V. G., Fournier, E., Isakoff, S. J., Skolnik, E. Y., and Lemmon, M. A. (2000) Structural basis for discrimination of 3-phosphoinositides by pleckstrin homology domains. *Mol. Cell 6*, 373–384.
32. Lietzke, S. E., Bose, S., Cronin, T., Klarlund, J., Chawla, A., Czech, M. P., and Lambright, D. G. (2000) Structural basis of 3-phosphoinositide recognition by pleckstrin homology domains. *Mol. Cell 6*, 385–394.
33. Corbin, J., Dirkx, R., and Falke, J. (2004) GRP1 pleckstrin homology domain: activation parameters and novel search mechanism for rare target lipid. *Biochemistry 43*, 16161–16173.
34. Schaefer, M., Albrecht, N., Hofmann, T., Gudermann, T., and Schultz, G. (2001) Diffusion-limited translocation mechanism of protein kinase C isotypes. *FASEB J. 15*, 1634–1636.
35. Chisari, M., Saini, D. K., Kalyanaraman, V., and Gautam, N. (2007) Shuttling of G protein subunits between the plasma membrane and intracellular membranes. *J. Biol. Chem. 282*, 24092–24098.
36. Saini, D. K., Kalyanaraman, V., Chisari, M., and Gautam, N. (2007) A family of G protein $\beta\gamma$ subunits translocate reversibly from the plasma membrane to endomembranes on receptor activation. *J. Biol. Chem. 282*, 24099–24108.
37. Kusumi, A., Nakada, C., Ritchie, K., Murase, K., Suzuki, K., Murakoshi, H., Kasai, R. S., Kondo, J., and Fujiwara, T. (2005) Paradigm shift of the plasma membrane concept from the two-dimensional continuum fluid to the partitioned fluid: High-speed single-molecule tracking of membrane molecules. *Annu. Rev. Biophys. Biomol. Struct. 34*, 351–378.
38. Arrio-Dupont, M., Foucault, G., Vacher, M., Devaux, P. F., and Cribier, S. (2000) Translational diffusion of globular proteins in the cytoplasm of cultured muscle cells. *Biophys. J. 78*, 901–907.
39. Swaminathan, R., Bicknese, S., Periasamy, N., and Verkman, A. S. (1996) Cytoplasmic viscosity near the cell plasma membrane: translational diffusion of a small fluorescent solute measured by total internal reflection-fluorescence photobleaching recovery. *Biophys. J. 71*, 1140–1151.
40. Jacobson, K., Hou, Y., Derzko, Z., Wojciesszyn, J., and Organisciak, D. (1981) Lipid lateral diffusion in the surface membrane of cells and in multibilayers formed from plasma membrane lipids. *Biochemistry 20*, 5268–5275.
41. Cho, H., Kim, Y. A., Yoon, J.-Y., Lee, D., Kim, J. H., Lee, S. H., and Ho, W.-K. (2005) Low mobility of phosphatidylinositol 4,5-bisphosphate underlies receptor specificity of Gq-mediated ion channel regulation in atrial myocytes. *Proc. Natl. Acad. Sci. USA 102*, 15241–15246.
42. Cho, H., Kim, Y. A., and Ho, W.-K. (2006) Phosphate number and acyl chain length determine the subcellular location and lateral mobility of phosphoinositides. *Mol. Cells 22*, 97–103.
43. Janetopoulos, C., Jin, T., and Devreotes, P. (2001) Receptor-mediated activation of heterotrimeric G-proteins in living cells. *Science 291*, 2408–2411.
44. Wright, L. P., and Philips, M. R. (2006) CAAX modification and membrane targeting of Ras. *J. Lipid Res. 47*, 883–891.
45. Lemmon, M. A., and Ferguson, K. M. (2000) Signal-dependent membrane targeting by pleckstrin homology (PH) domains. *Biochem. J. 350*, 1–18.
46. Hurley, J. H., and Grobler, J. A. (1997) Protein kinase C and phospholipase C: bilayer interactions and regulation. *Curr. Opin. Struct. Biol. 7*, 557–565.
47. Verdaguer, N., Corbalan-Garcia, S., Ochoa, W. F., Fita, I., and Gómez-Fernández, J. C. (1999) Ca(2+) bridges the C2 membrane-binding domain of protein kinase C α directly to phosphatidylserine. *EMBO. J. 18*, 6329–6338.
48. Pawson, T. (2004) Specificity in signal transduction: from phosphotyrosine-SH2 domain interactions to complex cellular systems. *Cell 116*, 191–203.

BI800596B